Nuclear levels and patterns of histone H3 modification and HP1 proteins after inhibition of histone deacetylases

Eva Bártová[1], Jiří Pacherník[2], Andrea Harničarová[1], Aleš Kovařík[1], Martina Kovaříková[1], Jirina Hofmanová[1], Magdalena Skalníková[3], Michal Kozubek[3] and Stanislav Kozubek[1,*]

[1]Institute of Biophysics, Academy of Sciences of the Czech Republic, Královopolská 135, 612 65, Brno, Czech Republic
[2]Center for Cell Therapy and Tissue Repair, Charles University, Vúvalu 84, 150 06 Prague 5, Czech Republic, and Laboratory of Molecular Embryology, Mendel University Brno, Zemědělská 1, 613 00 Brno, Czech Republic
[3]Faculty of Informatics, Masaryk University Brno, Botanická 68a, Czech Republic
*Author for correspondence (e-mail: kozubek@ibp.cz)

Accepted 03 August 2005
Journal of Cell Science 118, 5035-5046 Published by The Company of Biologists 2005
doi:10.1242/jcs.02621

Summary

The effects of the histone deacetylase inhibitors (HDACi) trichostatin A (TSA) and sodium butyrate (NaBt) were studied in A549, HT29 and FHC human cell lines. Global histone hyperacetylation, leading to decondensation of interphase chromatin, was characterized by an increase in H3(K9) and H3(K4) dimethylation and H3(K9) acetylation. The levels of all isoforms of heterochromatin protein, HP1, were reduced after HDAC inhibition. The observed changes in the protein levels were accompanied by changes in their interphase patterns. In control cells, H3(K9) acetylation and H3(K4) dimethylation were substantially reduced to a thin layer at the nuclear periphery, whereas TSA and NaBt caused the peripheral regions to become intensely acetylated at H3(K9) and dimethylated at H3(K4). The dispersed pattern of H3(K9) dimethylation was stable even at the nuclear periphery of HDACi-treated cells. After TSA and NaBt treatment, the HP1 proteins were repositioned more internally in the nucleus, being closely associated with interchromatin compartments, while centromeric heterochromatin was relocated closer to the nuclear periphery. These findings strongly suggest dissociation of HP1 proteins from peripherally located centromeres in a hyperacetylated and H3(K4) dimethylated environment. We conclude that inhibition of histone deacetylases caused dynamic reorganization of chromatin in parallel with changes in its epigenetic modifications.

Key words: Histone dimethylation, Histone acetylation, HP1 proteins, HDAC inhibitors, Nuclear periphery

Introduction

Post-translational modifications of amino-terminal histone tails are considered functionally important nuclear events that play a specific role in the dynamics of chromatin organization (Jenuwein and Allis, 2001; Dey et al., 2003). Histone methylation on different lysine residues, acetylation, phosphorylation, ubiquitination and polyADP-ribosylation (Mermoud et al., 2002; Lachner and Jenuwein, 2002) are related to epigenetic mechanisms regulating active and inactive chromatin states during the cell cycle, differentiation, cell death and malignant cell transformation. It is known that transcriptionally active regions of the genome are organized into euchromatic domains, and that silent loci form heterochromatic domains [summarised by Cremer and Cremer (Cremer and Cremer, 2001)].

Both heterochromatin and euchromatin are characterized by their specific histone methylation and acetylation patterns. Methylation of H3(K9), H3(K27) and H3(K20) are associated with the repressed chromatin state, whereas H3(K4), H3(K36) and H3(K79) methylation and/or histone acetylation have been correlated with active chromatin (see Fischle et al., 2003; Lachner et al., 2003). An example of a histone modification associated with heterochromatin is methylation of H3 at lysine 9 (K9) (Rea et al., 2000; Boggs et al., 2002; Mermoud et al., 2002; Peters et al., 2002; Lachner et al., 2003). This type of modification is mediated by histone methyltransferases (HMT) such as Suv39H1, which have the ability to catalyse H3(K9) methylation through their SET domain. In addition, this enzyme shares an evolutionarily conserved chromodomain with the specific heterochromatin protein 1 (HP1) (Rea et al., 2000; Rice and Allis, 2001). Transient binding of HP1 protein to chromatin, and its dynamic exchange, ensures the stability of heterochromatin domains, which has been confirmed in living cells (Cheutin et al., 2003). Mammalian non-histone HP1 proteins (α, β, γ isoforms) also play an important role in chromatin remodelling. HP1α and β associate with heterochromatin, while HP1γ localizes in both euchromatic and heterochromatic domains of interphase nuclei (Minc et al., 1999; Minc et al., 2000). HP1 function and related histone methylations influence the higher-order organization of active and inactive chromatin. This organisation is also regulated by acetylation that is catalysed by histone acetyltransferases (HATs) and removed by histone deacetylases (HDACs) (see Rice and Allis, 2001).

HDACs can be pharmacologically inhibited by trichostatin A (TSA) (Yoshida et al., 1990; Yoshida et al., 1995) or by

sodium butyrate (NaBt) (Bell and Jones, 1982; Hague at al., 1993; Koyama et al., 2000). At the cellular level, both these hyperacetylating agents produce cell-cycle arrest, differentiation and apoptosis (Barnard and Warwick, 1993; Koyama et al., 2000) (reviewed by Marks et al., 2001). Histone acetylation is often crucial in preparing the histone template for HMTs. For example, H3(K4) methylation, associated with active chromatin, is induced by HMT, which inhibits HDAC recruitment (Litt et al., 2001; Noma et al., 2001; Rice and Allis, 2001; Bernstein et al., 2002). In this way, an HMT such as yeast Set1 can probably mediate transcription by protecting active coding regions from deacetylation (Bernstein et al., 2002). Demethylation of H3(K4) by a nuclear homologue of amine oxidases (LSD1) has been described as a new mechanism involved in epigenetic modification of histones (Shi et al., 2004).

We have studied the effects of HDAC inhibitors on chromatin organization and its epigenetic modifications. The treatment of cells with HDAC inhibitors resulted in a number of cellular effects, including decondensation of chromatin, cell-cycle changes and induction of cell death by apoptosis in a fraction of the cell population. In addition, NaBt caused enterocytic differentiation of HT29 cells. Irrespective of the cellular processes induced, an increase in global levels of dimethylated H3(K9) and H3(K4) and acetylated H3(K9), and decreased levels of HP1 proteins, were found by western blotting. It seems that the nuclear periphery was particularly affected by HDAC inhibition. Both HDAC inhibitors changed peripheral H3(K9) into a strongly acetylated state, and H3(K4) into a dimethylated state, while the pattern of H3(K9) dimethylated regions was not affected. In addition, focally distributed HP1 proteins were redistributed closer to the nuclear interior, while centromeric heterochromatin was repositioned to the periphery. HP1 proteins of HDACi-treated cells were strongly associated with interchromatin compartments, which also suggested the dissociation of HP1 proteins from peripherally located (probably non-acrocentric) centromeres. Finally, we point out that treatment of cells with HDAC inhibitors caused substantial changes in histone modifications, accompanied by dynamic reorganization of chromatin. In spite of these changes in chromatin organization, the basic features of the radial arrangement of the genome (Sadoni et al., 1999; Skalníková et al., 2000; Kozubek, S. et al., 2002) are preserved.

Materials and Methods

Cell cultivation and treatments

Human small lung carcinoma cells A549 (ATCC) were plated at a density of 2×10^5/ml in Dulbecco's modified Eagle's medium (DMEM; PAN, Aidenbach, Germany) supplemented with 10% fetal calf serum, and the cells were treated the next day with the HDAC inhibitors trichostatin A (TSA, 75 nM; Sigma-Aldrich, Prague, Czech Republic) and sodium butyrate (NaBt, 5 mM; Sigma). Analyses were performed 48 hours after the HDAC inhibitor treatment. Human colon adenocarcinoma HT29 cells (ATCC) were also given TSA stimulation but at 25 nM concentration. The effects of NaBt were also studied in HT29 cells and in addition, the combination of NaBt with tumour necrosis factor α (TNFα) (Kovaříková et al., 2000) was tested. NaBt has the potential to induce differentiation of cells into enterocytes (Kovaříková et al., 2000). Twenty-four hours after plating, the cells were treated for 48 hours with NaBt (5 mM), TNFα (15 ng/ml) (Sigma), or a combination of the two. In order to compare differentiation of normal and tumour cells, the effect of NaBt was also studied in normal human embryonic colon FHC cells (ATCC) cultured in a mixture of Ham's F12 and DMEM (Sigma) containing Hepes (25 mM), cholera toxin (10 ng/ml), insulin (5 μg/ml), transferrin (5 μg/ml) and hydrocortisone (100 ng/ml), supplemented with 10% fetal calf serum (PAN). All cell lines studied were cultured in standard conditions at 37°C in a humidified atmosphere containing 5% CO_2.

Immunostaining of interphase nuclei

Cells were fixed with 4% formaldehyde for 10 minutes at room temperature (RT), permeabilized with 0.1% Triton X-100 for 3 minutes and with 0.1% saponin (Sigma) for 12 minutes, and washed twice in PBS for 15 minutes. They were then incubated for 1 hour at RT in 1% BSA dissolved in PBS. The slides were washed for 15 minutes in PBS, and cells were incubated with anti-dimethyl-histone H3 (Lys 9), anti-acetyl-histone H3 (Lys 9), anti-dimethyl-histone H3 (Lys 4); (cat. nos. 07-212; 06-942; 07-030), anti-HP1α (clone 15.19s2; no. 05-689), anti-HP1 β (no. 07-333), anti-HP1γ (clone 42s2, no. 05-690) and anti-CENP-A (no. 07-240). All antibodies were purchased from Upstate, Milton Keynes, UK. Each antibody was diluted 1:500 in 1% BSA dissolved in PBS, and then incubated overnight at 4°C. The cells were washed twice in PBS for 5 minutes and incubated for 1 hour with the appropriate fluorescein-conjugated secondary antibody [goat anti-rabbit IgG (no. F-0511), goat anti-mouse IgG (no. F-0257; Sigma) and Alexa Fluor 594 goat anti-mouse IgG_3; Molecular Probes], diluted 1:500 in 1% BSA dissolved in PBS. Immunostained cells were washed three times in PBS for 5 minutes, and DAPI (0.2 μg/ml) or TO-PRO-3 iodide (0.04 μg/ml, Molecular Probes, Invitrogen, KRD Ltd., Prague, Czech Republic) were used as counterstains. TO-PRO-3 has ability to stain both DNA and RNA and, therefore, nucleoli were strongly TO-PRO-3 positive. Nucleolar areas stained by TO-PRO-3 corresponded well to negative DAPI staining. When RNase treatment was used, TO-PRO-3 staining was absent in the nucleolar compartment. Nucleolar regions were easily distinguishable in both types of experiments with TO-PRO-3 counterstain.

Fluorescence in situ hybridisation applied after immunostaining (Immuno-FISH)

Cells were fixed in 4% formaldehyde in PBS for 10 minutes before immunostaining. After image acquisition of immunostained nuclei, the coordinates of the cells were written to the computer memory, the cells were washed in PBS, and post-fixed with 4% formaldehyde. The cells were washed again in PBS (three times for 4 minutes), permeabilized for 10 minutes in 0.2% saponin in PBS and washed in 0.2% Triton X-100 in PBS for 10 minutes. The slides were rinsed in 0.1 M Tris-HCl (pH 7.2) for 15 minutes and equilibrated in 20% glycerol in PBS for 20 minutes. Next, the slides were twice frozen in liquid nitrogen and thawed. The target DNA was denatured in 50% formamide in 2× SSC for 15 minutes at 75°C. Digoxigenin and/or biotinyl-labelled DNA probes were denatured prior to hybridisation, according to the manufacturer's instructions (Appligene Oncor, Gaithersburg, MD), and according to the hybridization solution used (Hybrisol VII, Oncor). We applied the following DNA probes: classical satellites of human chromosome (HSA) 9 (Oncor) and alpha satellites of HSA 8 and 10 (Oncor). Probes for the *MYC* gene (8q24.21 – clone RP11-440N18) and *CCND1* (11q13.3 – clone RP11-300I6) were prepared in our laboratory by propagation in *E. coli*, DNA isolation, nick translation and Cot-1 DNA application. The clones originated from the libraries of P. de Jong, kindly provided by Mariano Rocchi, University of Bari, Italy. The conditions for the hybridisation and post-hybridisation washing were selected according to the

manufacturer's instructions and/or in accordance with Bártová et al. (Bártová et al., 2000; Bártová et al., 2002).

Western blotting

Cells were washed with PBS and lysed in sodium dodecyl sulphate (SDS) lysis buffer (50 mM Tris-HCl, pH 7.5; 1% SDS; 10% glycerol). Protein concentrations were determined using the DC protein assay kit (Bio-Rad, Bio-Consult, Prague, Czech Republic). Lysates were supplemented with Bromophenol Blue (0.01%) and 1% β-mercaptoethanol, and equal amounts of total nuclear proteins (10 μg) were subjected to SDS-PAGE. Twelve percent polyacrylamide gel were used for analyses of all proteins studied. After being electrotransferred onto a polyvinylidene difluoride membrane (Immobilon-P, Sigma-Aldrich), proteins were immunodetected using appropriate primary and secondary antibodies, and visualized by ECL+Plus reagent (Amersham Pharmacia Biotech, Prague, Czech Republic) according to the manufacturer's instructions. The following primary antibodies were employed: antibodies against human dimethyl-histone H3 (Lys 9; no. 07-212, Upstate), anti-acetyl histone H3 (Lys 9; no. 06-942, Upstate), anti-dimethyl-histone H3 (Lys 4; no. 07-030, Upstate), anti-HP1α (clone 15.19s2; no. 05-689), anti-HP1β (no. 07-333) and anti-HP1γ (clone 42s2; no. 05-690). All these antibodies were purchased from Upstate. To verify the induction of apoptosis by HDACi, goat polyclonal antibody against the carboxyl terminus of mouse lamin B was used. This antibody (sc-6217, Santa Cruz Biotechnology, Santa Cruz, CA) crossreacts with the human homologue. The rabbit polyclonal antibody [PARP (H-250): sc-7150] against PARP protein of human origin was also used. PARP (H-250) reacts with PARP of mouse, rat and human origin. After immunodetection, each membrane was stained with Amido Black to confirm equal protein loading. Western blots were repeated two or three times on samples from independent experiments. In our experiments apoptosis was demonstrated not only by the presence of lamin B (45 kDa) and PARP (80 kDa) cleavage fragments, but early apoptosis was also detected by the TUNEL test as described by Bártová et al. (Bártová et al., 2003).

Flow-cytometric analyses of the cell cycle

Treated and untreated cells were washed twice in PBS and fixed for 30 minutes in 70% ethanol (–20°C). After repeated washing in PBS, the cells were stained with propidium iodide diluted to 10 μg/ml in Vindel's solution [1 mM Tris-HCl (pH 8.0), 1 mM NaCl, 0.1% Triton X-100, 10 μg/ml RNase A] for 30 minutes at 37°C. The cell-cycle profile was determined with a FACSCalibur flow cytometer (Becton Dickinson, Franklin Lakes, NJ) equipped with an argon-ion laser, using the 488 nm laser line for excitation. CellQuest software running on an Apple Macintosh computer connected to the flow cytometer was used for the data acquisition. The cell-cycle phases were analysed with the aid of ModFit software (Verity Software House, Topsham, ME).

Image acquisition and analyses

Images of immunostained cell nuclei were acquired using a confocal system consisting of an argon/krypton laser (Innova 70, Coherent) with an acousto-optical tuneable filter (AOTF, Brimrose) for wavelength selection, and a confocal head (QLC 100; VisiTech International, Sunderland, UK) connected to a Leica DMRXA epi-fluorescence microscope (Leica, Wetzlar, Germany) with a Piezo-controlled z-movement (Physik Instrumente, Lambda Photometrics, Harpenden, UK). The scanning system was driven by FISH 2.0 software (Kozubek et al., 1999) running on a PC computer. The images were captured with a fully programmable digital CoolSnap CCD camera (Photometrix, Tucson, AZ). The magnification of the objective lens was 100× (NA=1.3). The pixel/micron conversion factor was 15 pixels per micrometre. For adherent cells, 40 optical sections were scanned for each fluorochrome. In the case of quantitative immunocytochemistry, the fluorescence intensity was set optimally for control cells, and this exposure was retained for cells treated with HDACi in order to determine light intensity. Using FISH 2.0 software, the volumes of nuclei and changes in the volume of classical satellites of HSA 9 were calculated. In each optical section the area of the nucleus was determined, and a quantity proportional to the nuclear volume was further calculated from 40 optical sections as the sum of the section areas (S). The ratio of nuclear volumes in control and treated samples was calculated as S/Sc × 100%, where S was the value for the treated cells and Sc the value for the control cell population. Student's *t*-test was used for statistical analyses.

The distances of given genetic elements (classical satellites of HSA 9, alpha satellites of HSA 8 and 10, the *MYC* and *CCND1* genes and HP protein foci) from the nuclear weight centre, normalized to the local nuclear radius (R), were calculated in approximately 500 nuclei and averaged. The distances between homologous genetic elements, normalized to the average nuclear radius, were measured as additional parameters of nuclear topography. The distributions of fluorescence intensities across cell nuclei were determined using Andor iQ software (version 1.0.1 ANDOR Technology, South Windsor, CT). Student's *t*-test was used to calculate the significance of differences between distributions.

Results

HDAC inhibitors induce decondensation of interphase chromatin

In agreement with the known effect of TSA on chromatin [a decondensation in interphase nuclei (Tóth et al., 2004)], we observed an increase in the nuclear volume of A549 cells treated with TSA and NaBt (Fig. 1A). Compared with the control cell population, TSA caused an increase in the nuclear volume of approximately 56%, and NaBt of 43%. Similar effects, but to a different extent, were observed in HT29 cells treated with TSA, in which the nuclear volume was increased by 25% after TSA addition (Fig. 1A). When the HDACi-treated cells were cultured for 24 hour without inhibitors, the nuclear volume returned to control values (not shown). The HT29 cells differentiated by NaBt (Kovaříková et al., 2000) did not change their nuclear volume significantly (Fig. 1A), which may be associated with differentiation-dependent chromatin condensation, which in this case is induced in parallel with histone hyperacetylation. Chromatin decondensation was also induced by HDACi in the classical satellites of human chromosome 9 (Fig. 1B) where the volume of this region was enlarged up to 3.6-fold. In addition, increases in the distances between specific loci on the same chromosome were observed (see the last paragraph of the Results).

Inhibition of histone deacetylases is accompanied by the induction of apoptosis in a fraction of the cell population

Inhibitors of histone deacetylases also have an ability to induce cell death by apoptosis (Koyama et al., 2000; Tóth et al., 2004). In our experiments, in parallel with chromatin decondensation, a fraction of the A549 and HT29 cells (<20%) was induced to undergo apoptosis, which in contrast, is characterized by extensive chromatin compaction into apoptotic bodies. In these experiments, TSA appeared not only to be a more effective chromatin decondensation agent than NaBt (Fig. 1A), but also a more potent inducer of apoptosis, as shown by the presence of PARP (80 kDa) and lamin B (45 kDa) cleavage fragments,

which are more prominent after TSA treatment than after NaBt treatment (Fig. 1C). After HDACi treatment, terminally apoptotic cells detached from the culture dishes, but early apoptotic cells (5% according to the TUNEL test) were found in the adherent cell population. The fraction of early apoptotic cells, detected by the TUNEL test, was not included in immunocytochemical analyses.

Cell-cycle changes induced by HDACi

Flow cytometric analyses showed that TSA and NaBt induced specific changes in the cell-cycle profile. After TSA treatment, both A549 and HT29 cell lines were characterized by an increased number of cells in G2 phase (Fig. 2A) compared with control values. By contrast, NaBt induced progressive accumulation of cells in G1 phase of the cell cycle. In addition, after both TSA and NaBt treatments fewer S-phase cells were found. The apoptotic sub-G1 peak contributed to the adherent cell population by less than 5% and, therefore, it was not involved in cell cycle analyses. After HDACi treatment M phase represented less than 2% of the adherent population, as demonstrated microscopically.

Distinct histone modification levels and nuclear patterns induced by HDAC inhibitors in small lung carcinoma cells

The cytological changes observed in HDACi-treated cells were accompanied by an increase in global histone H3(K9) and H3(K4) dimethylation and H3(K9) acetylation (Fig. 2B). In addition, specific interphase patterns were found after inhibition of HDACs in the A549 cells (Fig. 3A,B,C, and quantification in D). In control cells, the H3(K9) dimethylated histones were homogeneously distributed in the interphase nuclei. H3(K9) dimethylation also appeared at the nuclear periphery and in the perinucleolar regions (Fig. 3A and see TO-PRO-3 staining in Materials and Methods). TSA- and NaBt-treated cells were also homogeneously immunostained by anti-dimethyl H3(K9) (Fig. 3A).

Interphase patterns of dimethylated H3(K4) and acetylated H3(K9) seem to be more dynamic than the pattern of histone H3(K9) dimethylation (Fig. 3B,C; compare with A and see the quantification in D). The nuclear periphery of control A549 cells contained a very small amount of histone H3 acetylated at K9 (Fig. 3B, white arrow) and the perinucleolar regions lacked H3(K9) acetylation (Fig. 3B, yellow arrows, and see TO-PRO-3 staining in Materials and Methods). After TSA treatment the cells became globally H3(K9) hyperacetylated, and many H3 histones in the nuclear periphery became acetylated [see Fig. 3D, acetyl H3(K9)–TSA]. In comparison with TSA stimulation, a slightly different interphase pattern was observed after NaBt treatment of A549 cells (Fig. 3B, NaBt). The nuclear periphery was not so densely H3(K9) acetylated as after TSA treatment. This observation supports our above-mentioned statement that NaBt is not as potent an agent for inducing histone hyperacetylation as TSA. After NaBt treatment, enhanced H3(K9) acetylation was also detected as an increased fluorescence intensity (Fig. 3B,D), however, two different nuclear regions without H3(K9) acetylation signals were found: perinucleolar regions (Fig. 3B, NaBt, yellow arrow, and see TO-PRO-3 staining in Materials and Methods) and large interchromatin compartments (Fig. 3B, NaBt, blue arrow).

Similarly to H3(K9) acetylation, dimethylation of histones H3 at K4 was mostly absent from a thin rim at the nuclear periphery of control cells, but this peripheral shell was not completely uniform (Fig. 3C, white arrow in control). The perinucleolar regions of control cells also lacked H3(K4) dimethylation (Fig. 3C, last line, yellow arrow). After both

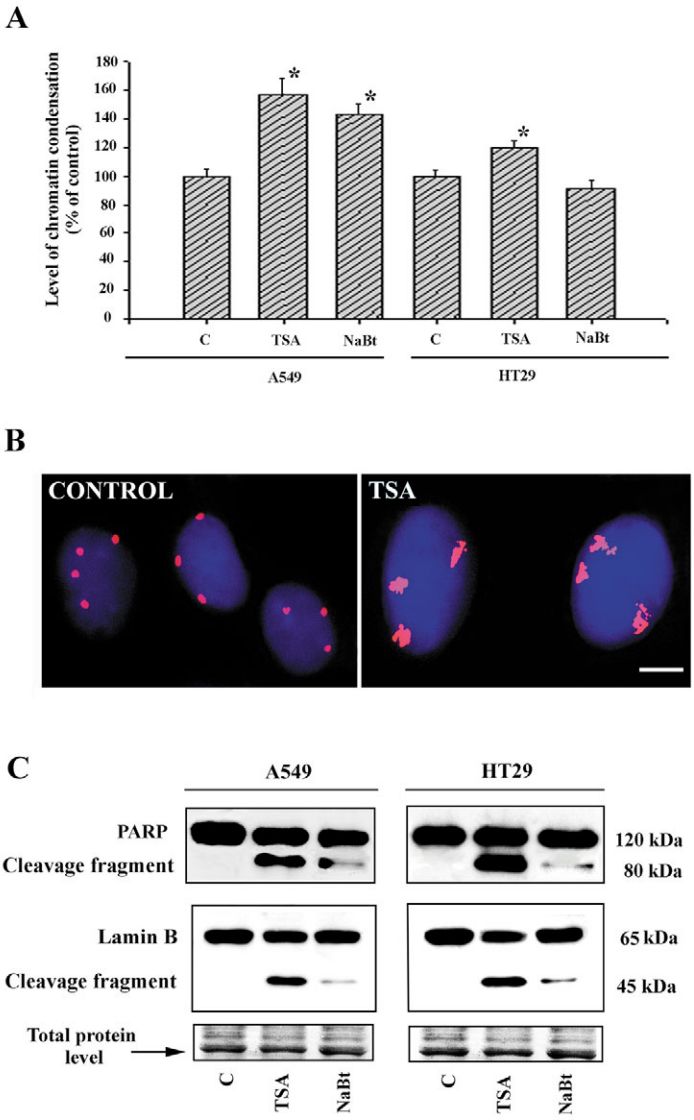

Fig. 1. (A) Changes in nuclear volume induced by HDACi (TSA and NaBt) determined in two human cell types (A549 and HT29). Average nuclear volume ± s.e.m. was calculated for each treatment and was related to the control values (100%). Asterisks indicate results significantly different from the control; $P<0.05$. (B) Chromatin decondensation of classical satellites of chromosome 9 in control and TSA-treated A549 cells. Bar, 2 μm. (C) The induction of apoptosis by HDACi was confirmed in A549 and HT29 cells by western blots that show the cleavage of PARP (120 kDa) into 80 kDa fragments and cleavage of lamin B (65 kDa) into 45 kDa fragments.

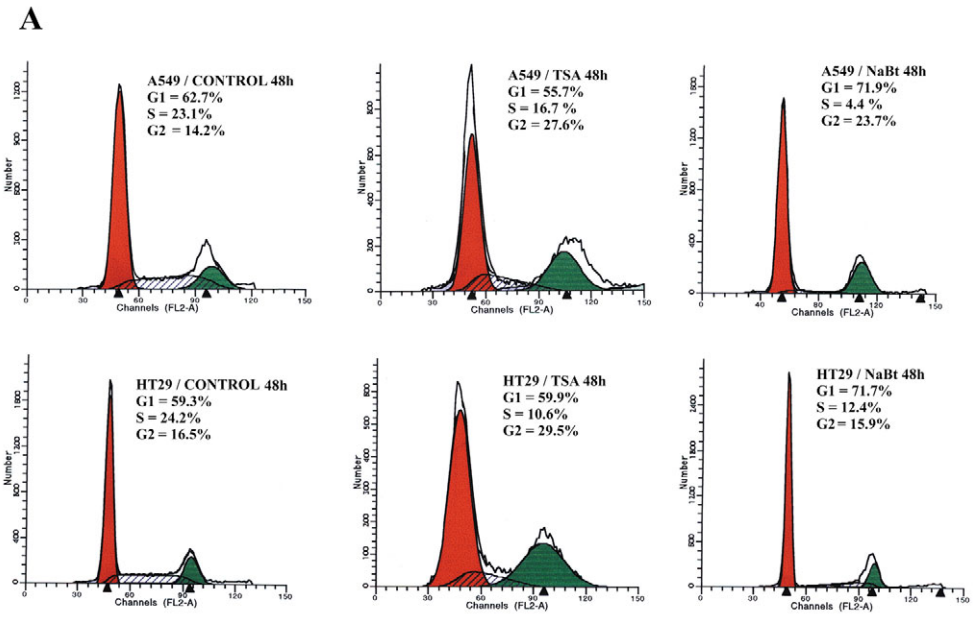

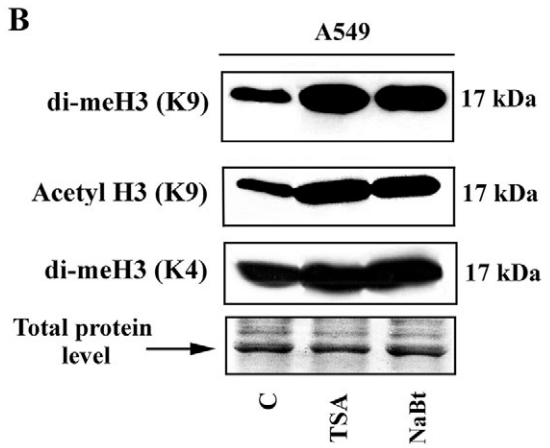

Fig. 2. (A) Flow cytometric detection of the cell-cycle profiles in TSA- and NaBt-treated A549 and HT29 cells. Modfit software analysis shows G1 (red), S (hatched) and G2 (green) stages of the cell cycle. NaBt induced accumulation of cells in G1 while TSA increased the number of cells in G2. (B) Western blot detection of dimethylated H3(K9) (17 kDa), acetylated H3(K9) (17 kDa) and dimethylated H3(K4) (17 kDa) in A549 cells treated with TSA and NaBt. The western blot data were related to the selected band (arrow) of total nuclear protein levels. The figures show an illustration of representative blots.

TSA and NaBt treatments of A549 cells, intense global staining by anti-dimethyl H3(K4) was observed, which was most pronounced at the nuclear periphery (Fig. 3C, white arrows for TSA and NaBt). The densely H3(K4) dimethylated peripheral shell of HDACi-treated cells was not fully intact (see red arrow in Fig. 3C as an example). In the nuclei of HDACi-treated cells, the perinucleolar regions continued to lack H3(K4) dimethylation (Fig. 3C, yellow arrows), and interchromatin compartments were visible (e.g. Fig. 3C, blue arrow). Quantitative immunocytochemistry revealed that the patterns of H3(K9) acetylation and H3(K4) dimethylation were more dynamic after HDACi treatment than patterns of H3(K9) dimethylation (Fig. 3D). In particular, the nuclear periphery underwent extensive changes in histone modifications (Fig. 3).

Distinct histone modification levels and nuclear patterns induced by HDAC inhibitors in colon cell lines

HDAC inhibitors such as sodium butyrate (NaBt) have been found to arrest cell growth and induce differentiation. In human colon adenocarcinoma HT29 cells, NaBt stimulates terminal enterocytic differentiation (Kovaříková et al., 2000). Using this experimental model, selected histone methylation states were analysed in our experiments. In comparison with the untreated control (Fig. 4A,C), NaBt increased the levels of dimethylated H3(K9), dimethylated H3(K4) and acetylated H3(K9), but to different extents (Fig. 4, NaBt). The most pronounced differences between control and treated cells were observed for H3(K9) acetylation (Fig. 4A). NaBt-mediated differentiation of HT29 cells can be partially inhibited by the addition of tumour necrosis factor α (TNFα) (Kovaříková et al., 2000). In our experiments, a combination of these drugs potentiated induction of apoptosis (compare the 45 kDa cleavage fragment of the NaBt sample with that of NaBt+TNF in Fig. 4A). This combined effect of NaBt+TNFα on cell differentiation and apoptosis was not reflected in changes in the levels of H3(K9) and H3(K4) dimethylation and H3(K9) acetylation (Fig. 4A). Levels of dimethylation and acetylation of histones H3 were increased after treatments with NaBt, independently of the influence of TNFα. TNFα did not itself change the levels of methylation and acetylation (Fig. 4A). In order to compare normal and malignant cell phenotypes, histone methylation and acetylation states were also studied during enterocytic differentiation of normal human embryonic colon cells (FHC). For both normal and malignant cells induced to differentiate into enterocytes, we observed identical changes in the histone modifications studied (compare Fig. 4A and B).

In additional experiments, the effects of both TSA and NaBt were tested and compared in HT29 cells. These experiments revealed identically increased levels of histone H3(K9) and H3(K4) dimethylation and H3(K9) acetylation (for comparison, the effects of TSA and NaBt on one gel are shown in Fig. 4C).

As in A549 cells, H3(K9) dimethylated regions were also homogenously dispersed in the nuclei of HT29 control cells. The increased levels of H3(K9) dimethylation induced by TSA and NaBt in HT29 cells (Fig. 4C) were not accompanied by changes in the nuclear pattern of this epigenetic modification

(Fig. 4D, top row). A pronounced increase in fluorescence intensity was found in HT29 cells stimulated with either TSA or NaBt after immunostaining with anti-acetyl H3(K9) (Fig. 4D, middle row). More densely stained nuclei appeared after TSA treatment than after NaBt cell stimulation. The H3(K9) acetylation pattern was characterized by visibly unstained

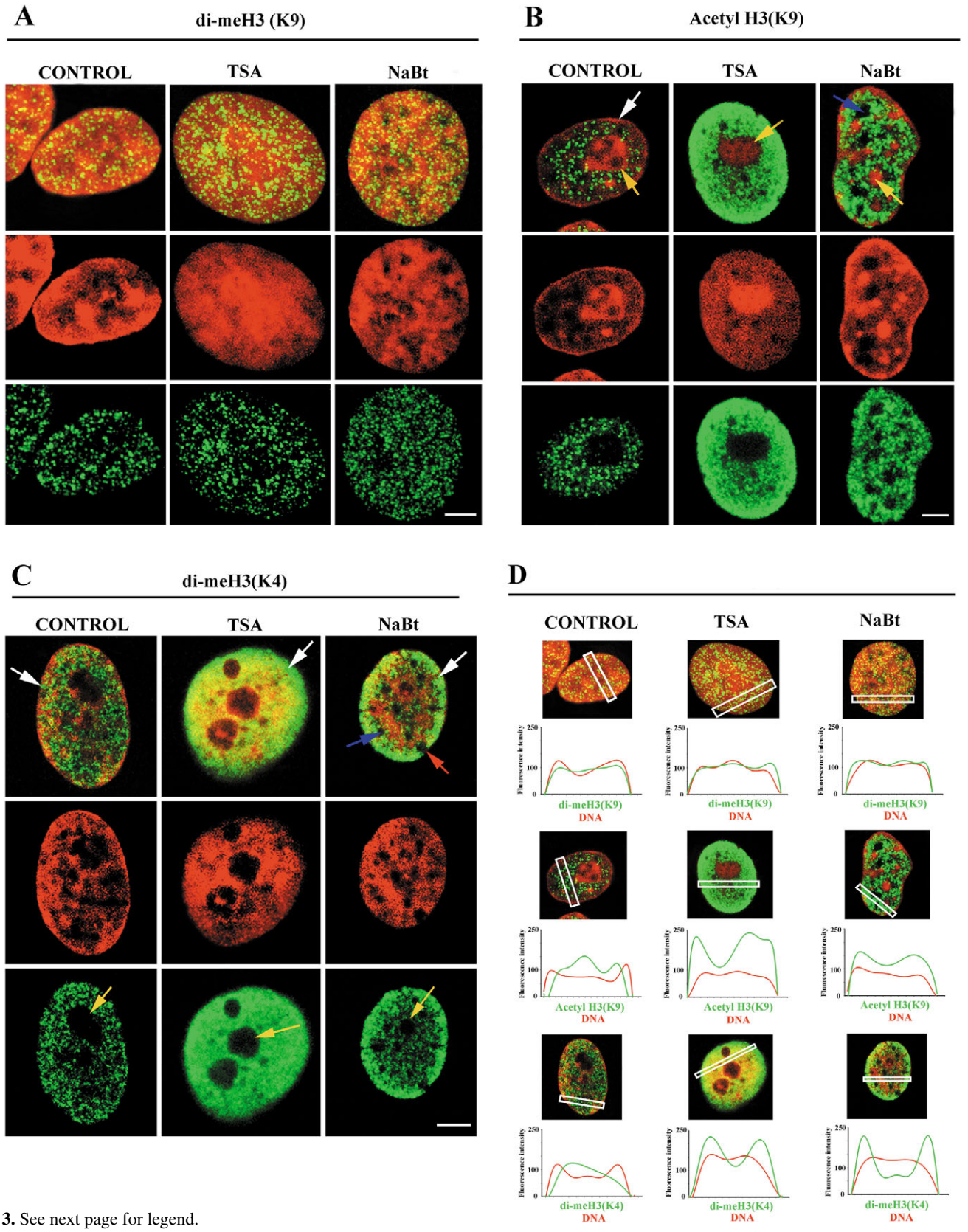

Fig. 3. See next page for legend.

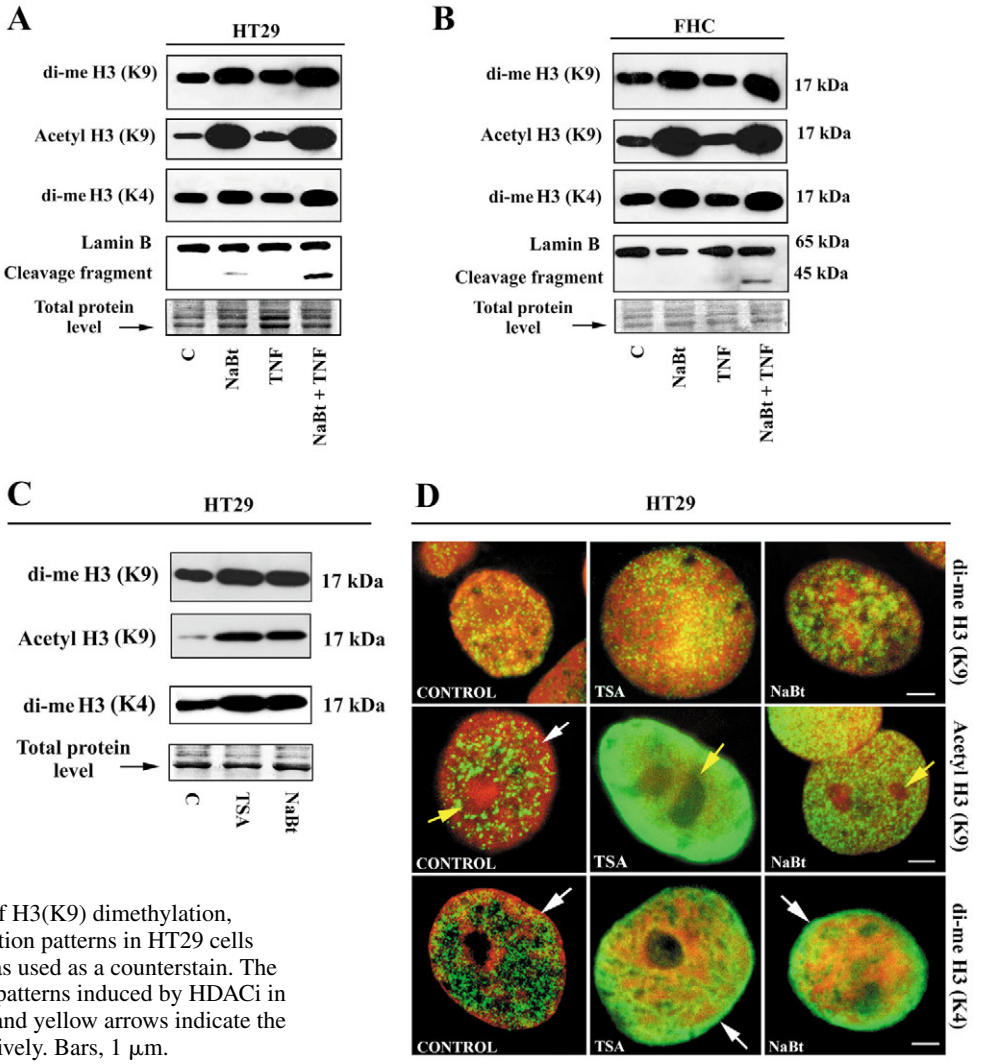

Fig. 4. The levels of H3(K9) dimethylation (17 kDa), H3(K9) acetylation (17 kDa) and H3(K4) dimethylation (17 kDa) analysed by western blots in (A) the human HT29 colon cancer cell line, and (B) normal colon cells FHC. In order to compare the effects of HDACi on normal and tumour cells, the following treatments were tested: sodium butyrate (HT29/NaBt; FHC/NaBt), TNFα (HT29/TNFα; FHC/TNFα) and a combination of NaBt with TNFα (HT29/NaBt+TNF; FHC/NaBt+TNF). In both cell types, in comparison with the control, there was a substantial increase in H3(K9) and H3(K4) dimethylation and H3(K9) acetylation after treatments involving NaBt. Apoptotic cleavage of lamin B (65 kDa) into a 45 kDa fragment was enhanced after the combined treatment with NaBt and TNFα (see A and B). Protein levels for all treatments were normalized to the selected band (arrow) of total nuclear protein levels.
(C) Comparison of the effects of TSA and NaBt on H3(K9) dimethylation (17 kDa), H3(K9) acetylation (17 kDa) and H3(K4) dimethylation (17 kDa) of HT29 cells. (D) Immunocytochemical analyses of H3(K9) dimethylation, H3(K9) acetylation and H3(K4) dimethylation patterns in HT29 cells treated with TSA and NaBt. TO-PRO-3 was used as a counterstain. The images represent the histone modification patterns induced by HDACi in the majority of the cell population. White and yellow arrows indicate the nuclear periphery and the nucleoli, respectively. Bars, 1 μm.

areas, probably representing nucleoli (Fig. 4D, middle row, yellow arrows), in contrast to the H3(K9) dimethylation that appeared at perinucleolar regions (Fig. 4D, top row). As observed in A549 cells, H3(K9) acetylation was extended at the nuclear periphery of HDACi-treated cells, while the absence of H3(K9) acetylation was also confirmed at the nuclear periphery of control cells (Fig. 4D, white arrow in control). A similar nuclear pattern was also observed for H3(K4) dimethylation, which was characterized by increased fluorescence intensity at the nuclear periphery of TSA- and NaBt-treated cells (Fig. 4D, bottom row, white arrows) while an absence of H3(K4) dimethylation at the nuclear periphery was found in control HT29 cells (Fig. 4D, di-meH3(K4), white arrow in control).

Fig. 3. Immunocytochemical analyses of (A) H3(K9) dimethylation, (B) H3(K9) acetylation and (C) H3(K4) dimethylation patterns in A549 cells treated with TSA or NaBt. (Top row) Overlays of TO-PRO-3 counterstained images (middle row) with immunocytochemical staining (bottom row). Nucleolar regions are indicated by yellow arrows, the nuclear periphery by white arrows, and interchromatin compartments by blue arrows. The red arrow in C indicates the non-uniform nature of the peripheral shell.
(D) Quantitative analysis of the distribution of H3(K9) dimethylation, H3(K9) acetylation and H3(K4) dimethylation across interphase nuclei. The fluorescence intensity was evaluated across the region indicated by the rectangle in each panel using Andor iQ software. The images represent the histone modification patterns induced by HDACi in the majority of the cell population. Bars, 1.5 μm.

HDAC inhibitors decrease the levels and change the interphase patterns of HP1 proteins

Using western blots, the levels of all isoforms (α, β, γ) of heterochromatin protein HP1 were studied. These analyses revealed decreased levels of HP1 proteins in A549 and HT29 cells treated with HDAC inhibitors (Fig. 5A). The most pronounced changes were observed for HP1γ in A549 cells treated with both HDACi, while HP1β levels were only slightly reduced (western blot panel in Fig. 5A).

The nuclear pattern of HP1 proteins (α, β, γ) in A549 cells treated with HDACi is shown in Fig. 5B. In these experiments it was observed that these proteins form specific foci in both the control and treated cells (Fig. 5B) but, the most distinct foci could be seen in HDACi-stimulated cells (Fig. 5B). In addition, the foci of all isoforms of HP1 proteins were located more interiorly in HDACi-treated cells than in control cells (Fig.

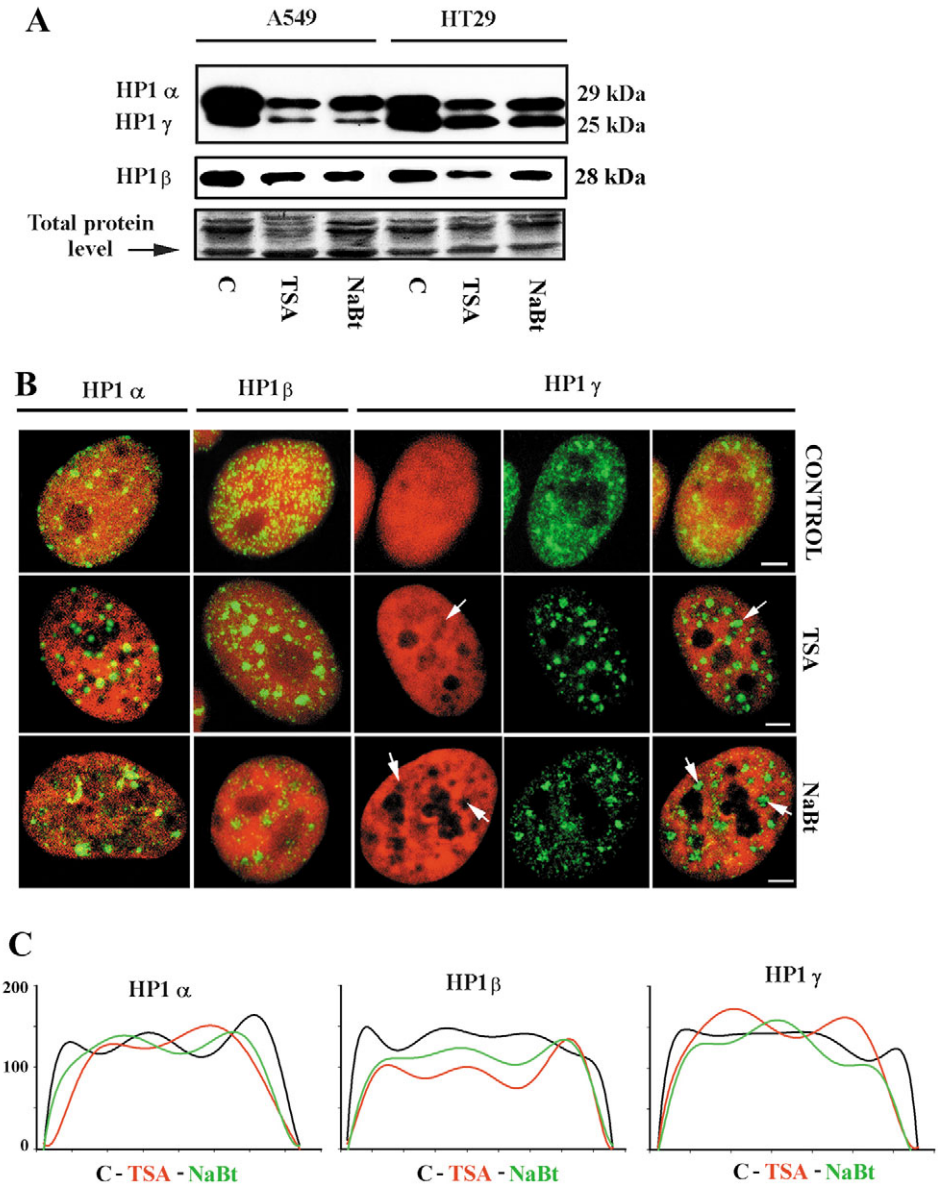

Fig. 5. (A) Western blot analyses of HP1α, β and γ proteins in A549 and HT29 cells treated with HDAC inhibitors. Protein levels for all treatments were normalized to the selected band (arrow) of total nuclear protein levels. (B) Interphase patterns of HP1α, β (overlays) and γ (counterstain, immunostaining and overlay) studied by immunocytochemistry in A549 cells treated with TSA and NaBt. In order to demonstrate the location of HP1γ in interchromatin compartments (white arrows) colour separations are also shown. Bars, 1 μm. (C) Nuclear radial distributions of HP1 foci (α, β, γ) in control (black line), TSA-treated cells (red line) and NaBt-treated cells (green line), showing the repositioning of HP1 proteins towards the nuclear interior. Average fluorescence intensities across the nucleus were determined using Andor iQ software.

5C). This central relocation of HP1 proteins was accompanied by repositioning of CENP-A regions (centromeric H3 variant) towards the nuclear periphery (Fig. 6A, Mid. confocal section), which confirmed the dissociation of HP1 from peripherally located centromeric heterochromatin (Fig. 6B). However, in our experimental system, some interiorly positioned centromeres remained associated with HP1α (Fig. 6B).

In the case of HP1γ it was demonstrated that the foci can be found in interchromatin compartments (ICs) of HDACi-treated cells (Fig. 5B, white arrows). The other two isoforms of this protein were also found in close association with ICs. Similar nuclear patterns of HP1 proteins were observed in HT29 cells treated with HDACi (not shown).

The influence of HDACi on the nuclear arrangement of heterochromatic regions and selected coding sequences

Because of the affinity of HP1 protein to centromeric heterochromatin, radial distributions of selected centromeres were investigated. The centre-of-nucleus to centromere average distances and centromere-to-centromere average distances, were analysed for human chromosomes 8, 9 and 10. For comparison, selected coding sequences (the *MYC* and *CCND1* genes) were also studied after HDACi treatment. The results show that centromeric heterochromatin was repositioned closer to the nuclear periphery, while coding regions were relocated closer to the nuclear centre (Table 1). Consistent with this observation, the distances between homologous centromeres were increased, and distances between homologous genes were decreased. The increase in the distance between the *MYC* gene (8q24) and the centromere of chromosome 8 (Table 1) confirmed the decondensation of chromatin induced during histone hyperacetylation described above.

Finally, we investigated the relationship of centromeric regions to densely H3(K4) dimethylated chromatin at the nuclear periphery of TSA-treated A549 cells (Fig. 7). We found that the centromeres are integrated into chromatin

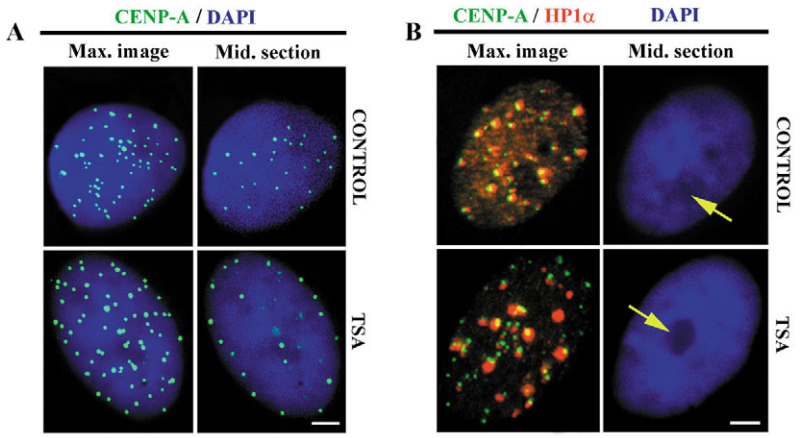

Fig. 6. (A) Nuclear patterns of CENP-A in maximum image (Max. image) and in a central section (Mid. section) for control and TSA-treated A549 cells, showing the repositioning of centromeres towards the nuclear periphery after HDACi treatment. Note that the peripheral location of CENP-A foci can be seen in the central section, which cannot be easily distinguished in the maximum image.
(B) Immunocytochemistry with anti-CENP-A and anti-HP1α in control and TSA-treated A549 cells. Co-localization of centromeres (green signals) with HP1α protein (red signals) was observed in the control cell population whereas TSA-induced dissociation of both regions, mostly at the nuclear periphery. DAPI was used as a counterstain; yellow arrows indicate the location of nucleoli. Bar, 1 μm.

compartments that lack H3(K4) dimethylation in both control and TSA-treated samples (Fig. 7, compare control with TSA confocal sections). Confocal sections S1 and S3 are shown in order to demonstrate that most of the centromeric regions in TSA-treated cells are located on the nuclear periphery, which cannot be easily distinguished in the maximum image (Fig. 7). Similar results were obtained for H3(K9) acetylation (not shown).

Discussion

Cytological changes induced by HDAC inhibitors

Histone deacetylases (HDACs) can be inhibited by short-chain fatty acids such as sodium butyrate (Bell and Jones, 1982; Hague et al., 1993) and hydroxamic acids (e.g. Trichostatin A) (Yoshida et al., 1990; Yoshida et al., 1995; Koyama et al., 2000). HDAC inhibitors have the potential to induce changes in the cell-cycle profile, differentiation, apoptosis and to modulate chromatin plasticity, facilitating protein/DNA interactions and thus transcriptional control (Cohen et al., 1999; Kovaříková et al., 2000; Yamashita et al., 2003; Tóth et al., 2004). Several reports have suggested that cells treated with these agents undergo apoptosis as a terminal event of cell differentiation, and that it is connected with induced histone hyperacetylation leading to transcriptional activation of specific loci (Candido et al., 1978; McCaffrey et al., 1997). However, down-regulated expression of other loci can be induced by treatment with NaBt (Heruth et al., 1993; Krupitza et al., 1995) or TSA (Takahashi et al., 1996).

The first marked effects of HDACi are changes in nuclear volume (Fig. 1A), which is most probably related to chromatin decondensation. A pronounced decondensation was also found for classical satellites of chromosome 9 (Fig. 1B). In our experiments the changes in nuclear volume were reversible (not shown), which was in agreement with the results of Tóth et al. (Tóth et al., 2004), who reported reversibility in chromatin decondensation after TSA treatment in HeLa cells.

An exception to the changes in nuclear volume was found in the case of NaBt treatment of HT29 cells (Fig. 1A), in which these effects were not significant, probably due to the fact that two processes were induced together: hyperacetylation, producing chromatin decondensation (Tóth et al., 2004), and cell differentiation, accompanied in most cases by chromatin compaction (Bártová et al., 2000; Francastel et al., 2000) (A.H. et al., unpublished data). These processes may antagonize nuclear volume changes that could also be the consequence of the cell-cycle effects. Therefore, cell-cycle profiles were monitored after

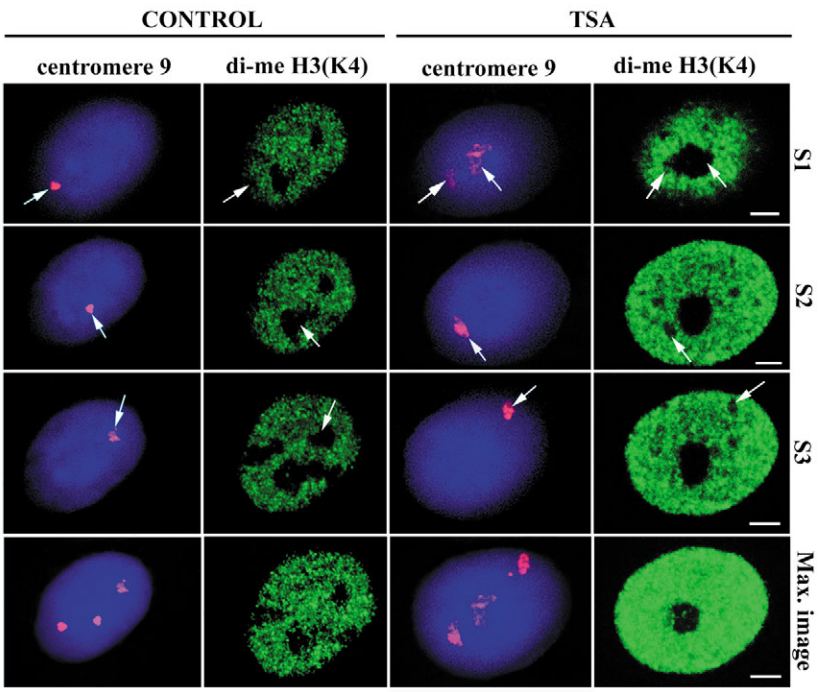

Fig. 7. Confocal sections of cell nuclei at different z-positions (S1, S2 and S3) and maximum images (bottom) are shown for nuclei of A549 cells. The H3(K4) dimethylation pattern (green signals) was determined by immunocytochemistry, and centromeric regions (classical satellites of chromosome 9; red signals) were stained using the FISH technique. In both control and TSA-treated cells the centromeres were located in regions lacking H3(K4) dimethylation. Bar, 1 μm.

Table 1. Rearrangement of selected centromeric loci and coding sequences in A549 cells treated and not treated with TSA

Locus	Untreated	TSA-treated
Centromeric heterochromatin		
9cen – 9cen/R	78.4±0.7%	83.3±0.8%*
Nuclear centre – 9cen/R	60.8±0.5%	62.3±0.5%*
8cen – 8cen/R	80.6±1.3%	91.6±1.9%*
Nuclear centre – 8cen/R	61.0±0.8%	67.1±1.0%*
10cen – 10cen/R	72.8±1.3%	82.8±1.6%*
Nuclear centre – 10cen/R	55.8±0.8%	62.9±1.2%*
Coding sequences		
MYC – MYC/R	91.9±1.4%	84.9±1.2%*
Nuclear centre – MYC/R	71.1±0.9%	68.8±0.5%*
CCND1 – CCND1	76.0±0.9%	73.3±1.0%
Nuclear centre – CCND1	60.5±0.4%	54.7±0.7%*

The distances of the given genetic element from the nuclear centre and distances between homologous genetic elements were analyzed.
Statistically significant at *$P<0.05$.

treatment of cells with TSA and NaBt (Fig. 2A). TSA induced increased number of cells in G2 phase, while NaBt arrested the cells in G1. Because of the possible contribution of G2 cells to the increased nuclear volume, the G1 and G2 cells were investigated separately after TSA treatment. In these experiments, the nuclear volumes of both G1 and G2 cells were approximately doubled, suggesting equal levels of decondensation in both stages of the cell cycle after HDAC inhibition.

In parallel with chromatin decondensation, a fraction of the cell population underwent apoptosis after HDACi treatment (Fig. 1C). In our experiments TSA was a more efficient pro-apoptotic agent than NaBt for both A549 and HT29 cells. Apoptosis, which was found in less than 20% of the total cell population studied (in both de-attached and adherent cells), is characterized by extensive chromatin compaction (Kerr et al., 1972; Cohen, 1994). The apoptotic cells were eliminated from our immunocytochemical analyses, as mentioned in the Results section. In order to elucidate the influence of apoptosis on histone methylation levels, additional experiments were performed with the exclusively pro-apoptotic agent etoposide, which does not change the level of H3(K9) dimethylation (see Bártová et al., 2005). We therefore assume that the apoptotic process was probably not responsible for increased H3(K9) dimethylation levels observed after HDACi treatment. This is also supported by the results shown in Fig. 4A,B, which demonstrate an identical increase in histone methylation and acetylation after NaBt alone or after simultaneous addition of NaBt and TNFα, which potentiates apoptosis (Fig. 4A,B, lamin B cleavage).

Changes of histone modifications and higher-order chromatin structure induced by HDAC inhibitors

The aim of our experiments was to demonstrate possible differences in selected modifications of histones, HP1 protein levels and nuclear patterns induced after treatment of cells with TSA and NaBt. Increased H3(K4) dimethylation and H3(K9) acetylation, and a constant level of H3(K9) dimethylation were expected after HDACi treatment. Stability of the H3(K9) dimethylation was expected because of the absence of the corresponding histone demethylases (Rice and Allis, 2001). However, on a global nuclear level, increased H3(K9) and H3(K4) dimethylation, as well as increased H3(K9) acetylation, were observed after TSA or NaBt treatment (Fig. 2B). These results strongly support the conclusion that H3(K9) acetylation and H3(K9) dimethylation occur in independent sets of H3 molecules, as reported by Maison et al. (Maison et al., 2002) for pericentric heterochromatin.

In our experiments, the significantly increased levels of histone modifications studied (Fig. 2B) were accompanied by changes in interphase patterns. The levels of the proteins determined by western blots do not always correspond to those determined by quantitative immunocytochemistry, which can be influenced to a greater extent by experimental conditions, such as accessibility of epitopes to antibodies. Therefore, the density of immunostaining may appear the same for both control and treated cells (Fig. 3A for H3(K9) dimethylation) in spite of the fact that western blots showed increased levels after HDACi (Fig. 2B).

In both control and treated cells, H3(K9) dimethylated histones were equally dispersed in interphase nuclei, including the perinucleolar regions (Fig. 3A). However, in control cells, H3(K9) acetylated and H3(K4) dimethylated histones were mostly absent from the nuclear periphery, and from the perinucleolar regions (Fig. 3B,C). After TSA and NaBt stimulation, peripheral histones became H3(K9)-acetylated and H3(K4)-dimethylated (Fig. 3B,C, and quantification in D). A similarly increased level of acetylation at the nuclear periphery in TSA-treated cells was also reported by Gilchrist et al. (Gilchrist et al., 2004) for H3 and H4 histones, while the nuclear pattern of H3(K9) dimethylation remained unchanged. In our experiments, we confirmed that these findings are also valid for another HDAC inhibitor, sodium butyrate, and therefore it seems to be a general effect caused by histone hyperacetylation. In addition, we observed that H3(K4) dimethylation, associated with the active chromatin state (summarised by Lachner et al., 2003), is also more pronounced at the nuclear periphery of cells treated with both hyperacetylating agents (Fig. 3C,D and Fig. 4D). The strongly acetylated and H3(K4) dimethylated peripheral shell of HDACi-treated cells is not uniform (Fig. 3B,C, red arrow, and Fig. 7). Uniformity is interrupted by centromeric heterochromatin (Fig. 7) that is characterized by pronounced reposition to the nuclear periphery of HDACi-treated cells (Table 1 and Fig. 6A).

These observations are in accordance with the radial arrangement of the genome in the nucleus; in which transcriptionally silent chromatin is located near the nuclear periphery and active loci are positioned more interiorly (Sadoni et al., 1999; Skalníková et al., 2000; Kozubek, S. et al., 2002). After the cell treatment by HDACi, the fraction of centromeric heterochromatin located in the nuclear periphery increased, whereas the coding sequences analysed were either repositioned towards the nuclear interior (Table 1) or retained in their original nuclear position (A.H. et al., unpublished data). These results indicate that the HDAC inhibition did not alter the spatial arrangement of euchromatin and heterochromatin in interphase nuclei but rather it caused their more distinct compartmentalization.

Changes in the interphase patterns and levels of HP1 proteins after HDACi treatment

We studied the global levels of HP1 proteins in our

experiments. It is known that HP1α and β associate with heterochromatin, and HP1γ localizes to both euchromatic and heterochromatic compartments of interphase nuclei (Minc et al., 1999; Minc et al., 2000). During interphase, all HP1 subtypes are localized to centromeric heterochromatin and to promyelocytic leukaemia (PML) nuclear bodies, but with different preferences (Hayakawa et al., 2003). The HP1 function is closely related to histone H3(K9) methylation (see Rice and Allis, 2001). The HDAC inhibitors used in our experiments decreased the levels of all isoforms of HP1 proteins (Fig. 5A); therefore, these data also indicate a close association between global histone hyperacetylation and reduced levels of HP1 isoforms. In both cell types tested, the decrease in HP1 levels was accompanied by the formation of more pronounced foci of these proteins (Fig. 5B).

More remarkable distinctions in the patterns of HP1 proteins were reported by Gilbert et al. (Gilbert et al., 2003), who found a loss of HP1s during differentiation of chicken erythrocytes; HP1s were also absent from erythrocytes of *Xenopus* and zebrafish. A reversible disruption of HP1 proteins from centromeric heterochromatin after HDAC inhibition was reported by Taddei et al. (Taddei et al., 2001). In our experiments, distinct foci of HP1 proteins of HDACi-treated cells were found in the interior of the nucleus (Fig. 5C), dissociated from peripherally localized centromeric heterochromatin, which was directly shown for HP1α and CENP-A in colocalization experiments (Fig. 6B). These nuclear events could be associated with a reduced level of HP1α (Fig. 5A) and with the formation of more interiorly located distinct foci of the protein studied (Fig. 5B,C). In our experimental system, dissociation of HP1α from centromeres was not observed in all cases; some centromeres (especially centromeres of acrocentric chromosomes, positioned in close proximity to nucleoli) did not lose their HP1α binding partner (Fig. 6B).

The changes in the binding efficiency of HP1 proteins after HDAC inhibition could also be reflected in the co-localization of HP1 proteins with TO-PRO-3-negative interchromatin compartments (IC) (e.g. Fig. 5B, white arrows for HP1γ). IC regions represent chromatin-free areas lined by chromatin domain surfaces (Bridger et al., 1998; Cremer and Cremer, 2001) (reviewed by Dundr and Misteli, 2001). Visser et al. (Visser et al., 2000) suggested that chromatin loops can expand into these spaces and that transcriptional and splicing factors freely occupy these IC regions. These data imply that nuclear positioning of HP1 proteins in close proximity to IC could probably be important for their nuclear function in HDACi-treated cells.

Concluding remarks

In our experiments, a clear correlation was observed between increases in H3(K9) acetylation and in H3(K4) dimethylation, and decreased levels of HP1 proteins induced by HDACi. Contrary to our expectation, the level of H3(K9) dimethylation was increased, which suggests some additional mechanism regulating this type of histone modification. Looking at the patterns, we can conclude that H3(K9) dimethylation is homogeneously distributed within interphase nuclei and conserved after histone hyperacetylation. By contrast, H3(K9) acetylation and H3(K4) dimethylation are more dynamic, particularly at the nuclear periphery where these types of histone modification are more abundant after the treatment with HDAC inhibitors. These epigenetic changes were accompanied by peripheral repositioning of large fraction of centromeric heterochromatin in parallel with central repositioning of HP1 proteins. Colocalization experiments showed directly that histone hyperacetylation caused dissociation of HP1 protein from centromeres, particularly from those located at the nuclear periphery.

The following grant agencies supported this work: Grant Agency of Academy of Sciences of CR (GAAV) 500040508, Grant Agency of Czech Republic (GAČR) 202/04/0907, Ministry of Health of CR (IGAMZ) 1A/8241-3, EU project LSHG-CT-2003-503441, GAAV IAA 5004306, GAČR 1P050C084, GAAV AVOZ50040507, Ministry of Education LC535, GAČR 202/03/D033.

References

Barnard, J. A. and Warwick, G. (1993). Butyrate rapidly induces growth inhibition and differentiation in HT-29 cells. *Cell Growth Differ.* **4**, 495-501.

Bártová, E., Kozubek, S., Kozubek, M., Jirsová, P., Lukášová, E., Skalníková, M., Cafourková, A. and Koutná, I. (2000). Nuclear topography of the *c-myc* gene in human leukemic cells. *Gene* **244**, 1-11.

Bártová, E., Kozubek, S., Jirsová, P., Kozubek, M., Gajová, H., Lukášová, E., Skalníková, M., Gaňová, A., Koutná, I. and Hausmann, M. (2002). Nuclear structure and gene activity in human differentiated cells. *J. Struct. Biol.* **139**, 76-89.

Bártová, E., Jirsová, P., Fojtová, M., Souček, K. and Kozubek, S. (2003). Chromosomal territory segmentation in apoptotic cells. *Cell. Mol. Life Sci.* **60**, 979-990.

Bártová, E., Harničarová, A., Pacherník, J. and Kozubek, S. (2005). Nuclear topography and expression of the BCR/ABL fusion gene and its protein level influenced by cell differentiation and RNA interference. *Leuk. Res.* **29**, 901-913.

Bell, P. A. and Jones, C. N. (1982). Cytotoxic effects of butyrate and other differentiation inducers on immature lymphoid cells. *Biochem. Biophys. Res. Commun.* **104**, 1202-1208.

Bernstein, B. E., Humphrey, E. L., Erlich, R. L., Schneider, R., Bouman, P., Liu, J. S., Kouzarides, T. and Schreiber, S. L. (2002). Methylation of histone H3 Lys 4 in coding regions of active genes. *Proc. Natl. Acad. Sci. USA* **99**, 8695-8700.

Boggs, B. A., Cheung, P., Heard, E., Spector, D. L., Chinault, A. C. and Allis, C. D. (2002). Differentially methylated forms of histone H3 show unique association patterns with inactive human X chromosomes. *Nat. Genet.* **30**, 73-76.

Bridger, J. M., Herrmann, H., Munkel, C. and Lichter, P. (1998). Identification of an interchromosomal compartment by polymerization of nuclear-targeted vimentin. *J. Cell Sci.* **111**, 1241-1253.

Candido, E. P., Reeves, R. and Davie, J. R. (1978). Sodium butyrate inhibits histone deacetylation in cultured cells. *Cell* **14**, 105-113.

Cheutin, T., McNairn, A. J., Jenuwein, T., Gilbert, D. M., Singh, P. B. and Misteli, T. (2003). Maintenance of stable heterochromatin domains by dynamic HP1 binding. *Science* **299**, 721-725.

Cohen, E., Ophir, I. and Shaul, Y. B. (1999). Induced differentiation in HT29, a human colon adenocarcinoma cell line. *J. Cell Sci.* **112**, 2657-2666.

Cohen, J. J. (1994). Apoptosis: physiologic cell death. *J. Lab. Clin. Med.* **124**, 761-765.

Cremer, T. and Cremer, C. (2001). Chromosome territories, nuclear architecture and gene regulation in mammalian cells. *Nat. Rev. Genet.* **2**, 292-301.

Dey, A., Chitsaz, F., Abbasi, A., Misteli, T. and Ozato, K. (2003). The double bromodomain protein Brd4 binds to acetylated chromatin during interphase and mitosis. *Proc. Natl. Acad. Sci. USA* **100**, 8758-8763.

Dundr, M. and Misteli, T. (2001). Functional architecture in the cell nucleus. *Biochem. J.* **356**, 297-310.

Fischle, W., Wang, Y. and Allis, C. D. (2003). Extending the histone code: Modification cassettes and switches. *Nature* **425**, 475-479.

Francastel, C., Schübeler, D., Martin, D. I. K. and Groudine, M. (2000). Nuclear compartmentalization and gene activity. *Nat. Rev. Mol. Cell. Biol.* **1**, 137-143.

Gilbert, N., Boyle, S., Sutherland, H., de Las Heras, J., Allan, J., Jenuwein, T. and Bickmore, W. A. (2003). Formation of facultative heterochromatin in the absence of HP1. *EMBO J.* **22**, 5540-5550.

Gilchrist, S., Gilbert, N., Perry, P. and Bickmore, W. A. (2004). Nuclear organization of centromeric domains is not perturbed by inhibition of histone deacetylases. *Chromosome Res.* **12**, 505-516.

Hague, A., Manning, A. M., Hanlon, K. A., Huschtscha, L. I., Hart, D. and Paraskeva, C. (1993). Sodium butyrate induces apoptosis in human colonic tumour cell lines in a p53-independent pathway: implications for the possible role of dietary fibre in the prevention of large-bowel cancer. *Int. J. Cancer* **55**, 498-505.

Hayakawa, T., Haraguchi, T., Masumoto, H. and Hiraoka, Y. (2003). Cell cycle behavior of human HP1 subtypes: distinct molecular domains of HP1 are required for their centromeric localization during interphase and metaphase. *J. Cell Sci.* **116**, 3327-3338.

Heruth, D. P., Zirnstein, G. W., Bradley, J. F. and Rothberg, P. G. (1993). Sodium butyrate causes an increase in the block to transcriptional elongation in the *c-myc* gene in SW837 rectal carcinoma cells. *J. Biol. Chem.* **268**, 20466-20472.

Jenuwein, T. and Allis, C. D. (2001). Translating the histone code. *Science* **293**, 1074-1080.

Kerr, J. F., Wyllie, A. H. and Currie, A. R. (1972). Apoptosis: a basic biological phenomenon with wide-ranging implications in tissue kinetics. *Br. J. Cancer* **26**, 239-257.

Kovaříková, M., Pacherník, J., Hofmanová, J., Zadák, Z. and Kozubík, A. (2000). TNF-alpha modulates the differentiation induced by butyrate in the HT29 human colon adenocarcinoma cell line. *Eur. J. Cancer* **36**, 1844-1852.

Koyama, Y., Adachi, M., Sekiya, M., Takekawa, M. and Imai, K. (2000). Histone deacetylase inhibitors suppress IL-2-mediated gene expression prior to induction of apoptosis. *Blood* **96**, 490-495.

Kozubek, M., Kozubek, S., Lukášová, E., Marečková, A., Bártová, E., Skalníková, M. and Jergová, A. (1999). High-resolution cytometry of FISH dots in interphase cell nuclei. *Cytometry* **36**, 279-293.

Kozubek, S., Lukášová, E., Jirsová, P., Koutná, I., Kozubek, M., Gaňová, A, Bártová, E., Falk, M. and Paseková, R. (2002). 3D Structure of the human genome: order in randomness. *Chromosoma* **111**, 321-331.

Krupitza, G., Harant, H., Dittrich, E., Szekeres, T., Huber, H. and Dittrich, C. (1995). Sodium butyrate inhibits *c-myc* splicing and interferes with signal transduction in ovarian carcinoma cells. *Carcinogenesis* **16**, 1199-1205.

Lachner, M. and Jenuwein, T. (2002). The many faces of histone lysine methylation. *Curr. Opin. Cell Biol.* **14**, 286-298.

Lachner, M., O'Sullivan, R. J. and Jenuwein, T. (2003). An epigenetic road map for histone lysine methylation. *J. Cell Sci.* **116**, 2117-2124.

Litt, M. D., Simpson, M., Gaszner, M., Allis, C. D. and Felsenfeld, G. (2001). Correlation between histone lysine methylation and developmental changes at the chicken beta-globin locus. *Science* **293**, 2453-2455.

Maison, C., Bailly, D., Peters, A. H., Quivy, J. P., Roche, D., Taddei, A., Lachner, M., Jenuwein, T. and Almouzni, G. (2002). Higher-order structure in pericentric heterochromatin involves a distinct pattern of histone modification and an RNA component. *Nat. Genet.* **30**, 329-334.

Marks, P., Rifkind, R. A., Richon, V. M., Breslow, R., Miller, T. and Kelly, W. K. (2001). Histone deacetylases and cancer: causes and therapies. *Nat. Rev. Cancer* **1**, 194-202.

McCaffrey, P. G., Newsome, D. A., Fibach, E., Yoshida, M. and Su, M. S. (1997). Induction of gamma-globin by histone deacetylase inhibitors. *Blood* **90**, 2075-2083.

Mermoud, J. E., Popova, B., Peters, A. H., Jenuwein, T. and Brockdorff, N. (2002). Histone H3 lysine 9 methylation occurs rapidly at the onset of random X chromosome inactivation. *Curr. Biol.* **12**, 247-251.

Minc, E., Allory, Y., Worman, H. J., Courvalin, J. C. and Buendia, B. (1999). Localization and phosphorylation of HP1 proteins during the cell cycle in mammalian cells. *Chromosoma* **108**, 220-234.

Minc, E., Courvalin, J. C. and Buendia, B. (2000). HP1gamma associates with euchromatin and heterochromatin in mammalian nuclei and chromosomes. *Cytogenet. Cell Genet.* **90**, 279-284.

Noma, K., Allis, C. D. and Grewal, S. I. (2001). Transitions in distinct histone H3 methylation patterns at the heterochromatin domain boundaries. *Science* **293**, 1150-1155.

Peters, A. H., Mermoud, J. E., O'Carroll, D., Pagani, M., Schweizer, D., Brockdorff, N. and Jenuwein, T. (2002). Histone H3 lysine 9 methylation is an epigenetic imprint of facultative heterochromatin. *Nat. Genet.* **30**, 77-80.

Rea, S., Eisenhaber, F., O'Carroll, D., Strahl, B. D., Sun, Z. W., Schmid, M., Opravil, S., Mechtler, K., Ponting, C. P., Allis, C. D. and Jenuwein, T. (2000). Regulation of chromatin structure by site-specific histone H3 methyltransferases. *Nature* **406**, 593-599.

Rice, J. C. and Allis, C. D. (2001). Histone methylation versus histone acetylation: new insights into epigenetic regulation. *Curr. Opin. Cell Biol.* **13**, 263-273.

Sadoni, N., Langer, S., Fauth, C., Bernardi, G., Cremer, T., Turner, B. M. and Zink, D. (1999). Nuclear organization of mammalian genomes. Polar chromosome territories build up functionally distinct higher order compartments. *J. Cell Biol.* **146**, 1211-1226.

Shi, Y. J., Lan, F., Matson, C., Mulligan, P., Whetstine, J. R., Cole, P. A., Casero, R. A. and Shi, Y. (2004). Histone demethylation mediated by the nuclear arnine oxidase homolog LSD1. *Cell* **119**, 941-953.

Skalníková, M., Kozubek, S., Lukášová, E., Bártová, E., Jirsová, P., Cafourková, A., Koutná, I. and Kozubek, M. (2000). Spatial arrangement of genes, centromeres and chromosomes in human blood cell nuclei and its changes during the cell cycle, differentiation and after irradiation. *Chromosome Res.* **8**, 487-499.

Taddei, A., Maison, C., Roche, D. and Almouzni, G. (2001). Reversible disruption of pericentric heterochromatin and centromere function by inhibiting deacetylases. *Nat. Cell Biol.* **3**, 114-120.

Takahashi, I., Miyaji, H., Yoshida, T., Sato, S. and Mizukami, T. (1996). Selective inhibition of IL-2 gene expression by Trichostatin A, a potent inhibitor of mammalian histone deacetylase. *J. Antibiot.* **49**, 453-457.

Tóth, K. F., Knoch, T. A., Wachsmuth, M., Frank-Stohr, M., Stohr, M., Bacher, C. P., Muller, G. and Rippe, K. (2004). Trichostatin A-induced histone acetylation causes decondensation of interphase chromatin. *J. Cell Sci.* **15**, 4277-4287.

Visser, A. E., Jaunin, F., Fakan, S. and Aten, J. A. (2000). High resolution analysis of interphase chromosome domains. *J. Cell Sci.* **113**, 2585-2593.

Yamashita, Y., Shimada, M., Harimoto, N., Rikimaru, T., Shirabe, K., Tanaka, S. and Sugimachi, K. (2003). Histone, deacetylase inhibitor Trichostatin A induces cell-cycle arrest/apoptosis and hepatocyte differentiation in human hepatoma cells. *Int. J. Cancer* **103**, 572-576.

Yoshida, M., Hoshikawa, Y., Koseki, K., Mori, K. and Beppu, T. (1990). Structural specificity for biological activity of trichostatin A, a specific inhibitor of mammalian cell cycle with potent differentiation-inducing activity in Friend leukemia cells. *J. Antibiot.* **43**, 1101-1106.

Yoshida, M., Horinouchi, S. and Beppu, T. (1995). Trichostatin A and trapoxin: novel chemical probes for the role of histone acetylation in chromatin structure and function. *BioEssays* **117**, 423-430.